

# Internal variability of the Southern Ocean carbon sink in MPI-ESM large ensemble simulations: assessment of westerly wind changes

Aaron Spring

March 28, 2017

## Contents

<b>1</b>	<b>Introduction</b>	<b>3</b>
<b>2</b>	<b>Methods</b>	<b>4</b>
2.1	Model description . . . . .	4
2.2	Large ensemble . . . . .	7
2.3	Data . . . . .	8
<b>3</b>	<b>Historical evolution of the Southern Ocean carbon sink</b>	<b>9</b>
<b>4</b>	<b>Spatial distribution of Southern Ocean carbon sink</b>	<b>11</b>
4.1	Negative trends in carbon sink . . . . .	14
4.1.1	Changes in biology in negative CO <sub>2</sub> flux trends . . . . .	14
4.1.2	Changes in ocean circulation in negative CO <sub>2</sub> flux trends . . . . .	17
4.2	Positive trends in carbon sink . . . . .	18
4.2.1	Changes in biology in positive CO <sub>2</sub> flux trends . . . . .	19
4.2.2	Changes in ocean circulation in positive CO <sub>2</sub> flux trends . . . . .	21
<b>5</b>	<b>50-60S dominates Internal Variability of the total Southern Ocean carbon sink due to winds - need a better title: emphasis on 50S as driving int var region via winds</b>	<b>22</b>
<b>6</b>	<b>estimate: bio vs upwelling</b>	<b>23</b>
<b>7</b>	<b>Discussion</b>	<b>24</b>



# 1 Introduction

**why Southern Ocean is important** carbon budget oceanic uptake [Sabine et al., 2004] [Le Quéré et al., 2016] SO as constraint to reduce model uncertainties [Kessler and Tjiputra, 2016]

**Southern Ocean observations and call for models** Observation-based estimates report a large variability in the Southern Ocean carbon sink [Le Quéré et al., 2007, Landschützer et al., 2015]. Sparse observational data lack the ability to show the dynamics of internally varying processes, which demands for the evaluation with models.

**Hypothesis** The Southern Annular Mode (SAM), characterizing the strength and position of the westerly winds, is known to be the dominant mode of climate variability in the Southern hemisphere [Thompson and Wallace, 2000]. Supposing the strength and position of the westerlies winds as the major reason for climate variability for the Southern Ocean, how does the carbon system respond? Strengthening westerlies increase upwelling, so more carbon-rich waters entrain the upper ocean and hence outgas. This upwelling also brings additional nutrients for the deep ocean, which might foster primary production. However, if the wind mixes too strong though, primary production decreases because of light limitation [Sverdrup, 1953] or other physical controls of biological production.

**Previous studies on co2flux mechanism and trends, modelling and observations**  
Previous modeling studies were studying the impact of SAM on the carbon sink [Lovenduski et al., 2007, Hauck et al., 2013] or long-term carbon trends [Wang and Moore, 2012] using ocean-only models with atmospheric historic forcing. biology response on SAM [Lovenduski and Gruber, 2005]

**what's new?** coupled model for internal variability study: are ensembles able to reproduce decadal trends? CESM ICLE doesnt; Int. Var. co2flux controls in HAMOCC

**What I do and research questions** By using a large ensemble simulation based on the Max-Planck-Institute Earth System Model (MPI-ESM), I investigate the variability of the oceanic carbon uptake. I try to answer the following questions:

1. How large is the modeled internal variability of the Southern Ocean carbon sink?
2. Do I find similar trends to those observed in the 1990s and 2000s in a large ensemble?
3. How does variability in physical processes influence the carbon sink?

## 2 Methods

### 2.1 Model description

**listing MPI-ESM components** The MPI-ESM version 1.1.00p2<sup>1</sup> with a low-resolution configuration (MPI-ESM-LR) is used for the large ensemble simulations [Giorgetta et al., 2013]. The atmosphere component ECHAM6.3 runs on a T63 grid, corresponding to  $1.9^\circ$  horizontal resolution, with 47 vertical layers up to 0.01 hPa [Stevens et al., 2013]. Atmospheric pCO<sub>2</sub> levels are prescribed due to the CMIP5 protocol and well mixed [Taylor et al., 2012]. The carbon cycle is not coupled, so called diagnostic, so effects of changes in the terrestrial or oceanic carbon sink are not reflected in the atmospheric pCO<sub>2,atm</sub>. Since there is no biogeochemical riverine exchange, terrestrial and oceanic carbon sink do not interact (Fig. 1). The ocean component MPI Ocean Model (MPIOM) has a horizontal resolution of  $1.5^\circ$  on average, relating to a spatial resolution of 150km at  $30^\circ\text{S}$  and 40km in Antarctic coastal waters, and 40 fixed-depth vertical levels [Jungclaus et al., 2013]. The Hamburg Ocean Carbon Cycle Model (HAMOCC) represents the ocean biogeochemistry component and aims to describe the carbon cycle (Fig. 2) [Ilyina et al., 2013].

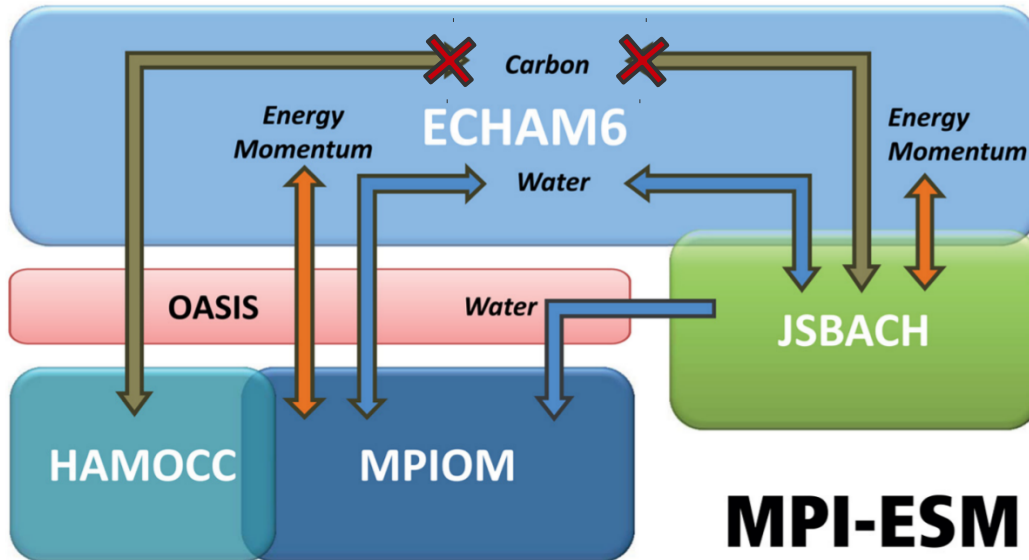


Figure 1: Schematic overview on the different components in MPI-Earth-System-Model with a diagnostic carbon cycle [Giorgetta et al., 2013]

<sup>1</sup>full source code: <https://code.zmaw.de/projects/mpi-esm/repository/show/tags/mpiesm-1.1.00p2>

I briefly explain how processes affecting the carbon cycle are implemented and subject to internal variability

**HAMOCC coupling** HAMOCC is coupled to ECHAM6 for exchange of atmospheric gases, precipitation and energy, e.g. heat as radiation and mechanical energy as wind stress. The required state variables required for HAMOCC, such as sea-ice cover, temperature T, salinity S and advective velocities  $\vec{v}$ , are provided from MPIOM.

**CO<sub>2</sub>flux description** The CO<sub>2</sub>flux implemented in earth-system models follow an empirical relationship following the conceptual one-layer stagnant film model ansatz of gas transfer velocity  $k$  [Wanninkhof, 1992]:

$$\begin{aligned} CO_2\text{flux} &= (1 - f)k\Delta pCO_2 \\ k &= 0.31u^2(Sc/660)^{-1/2} \\ \Delta pCO_2 &= pCO_{2,\text{atm}} - pCO_{2,\text{ocean}}, \end{aligned}$$

where  $f$  is the the sea-ice fraction of the grid cell,  $u$  wind speed, Sc Schmidt number, 660 is the Schmidt number of CO<sub>2</sub> in seawater at 20°C, and  $\Delta pCO_2$  the difference between the partial pressure of CO<sub>2</sub> in the atmosphere and ocean, so positive values of CO<sub>2</sub>flux represent a net flux from the ocean to the atmosphere. The potential partial pressure of CO<sub>2</sub> in water pCO<sub>2,ocean</sub> is solubility dependent by Henry's law and calculated according to [Weiss, 1974]. The potential of water to hold pCO<sub>2</sub> gives rise to the solubility pump of carbon [Volk and Hoffert, 1985]: cold waters hold exponentially more pCO<sub>2</sub> than warm waters and equatorial upwelling waters are warm and deep-water formation sites at high latitudes are cold.

**biology** In the euphotic zone upto a depth of 90m, primary production can convert nutrients, e.g. phosphate ( $PO_4$ ), nitrate ( $NO_3$ ), and iron, and inorganic carbon to organic matter by photosynthesis. The predator-prey relationship in HAMOCC follows a NPZD model [Six and Maier-Reimer, 1996]. Phytoplankton proliferate from nutrient consumption, zooplankton from phytoplankton consumption while detritus is left over as dead particulate organic material and sinks down the water column, a process refered to as the biological pump [Volk and Hoffert, 1985]. Primary production is parametrized by bulk phytoplankton which mimics diatom's, cocolithophore's and dinoflagellate's combined growth under exponentially increasing optimum growth rate temperatures [Eppley, 1972]. A lack of nutrients diminishes phytoplankton growth. The P-I saturation curve with a half-saturation constant serves as a nutrient limitation function [Smith, 1936]. Iron enters the water column via dust input climatology.

**Variability in biology** Biological processes are strongly dependent on physical properties of the ocean circulation. Mixing can change the nutrient supply, when remineralized nutrients from the deep ocean mix into the eutrophic zone. Mixing can also pull the

standing stock of phytoplankton deeper into the ocean where less light is available which inhibits growth. Changes in sea surface temperature also directly affect phytoplankton growth. Changes in ocean physics can lead to variability in biology. Also the atmosphere alters biological production: Cloud-cover reduces photosynthetic active radiation and freshwater fluxes can dilute nutrient concentrations.

**relevant MPIOM info: upwelling/advection/mixing** While detritus sinks to the ocean floor, it partly remineralizes and gives rise to high nutrient and DIC concentrations. Those tracers get advected by the Navier-Stokes equations with Boussinesq approximation in MPIOM [Marsland et al., 2003]. In areas of large scale upwelling such as the Southern Ocean those tracers can be advected to the ocean surface. Those carbon-rich waters then equilibrate with atmospheric pCO<sub>2</sub>. Upwelling processes are largely driven by divergency due to winds. The Southern Ocean westerly winds are variable in strength and location which is described by the Southern Annular Mode (SAM) index [Gong and Wang, 1999]. Ocean currents possess eddies which additionally mix the water column horizontally and vertically. As MPIOM's grid resolution doesn't permit eddies, they are parametrized [Gent et al., 1995]. Therefore the vertical mixing and diffusion based on Richardson-number dependent formulation is important for vertical gradients [Pacanowski and Philander, 1981].

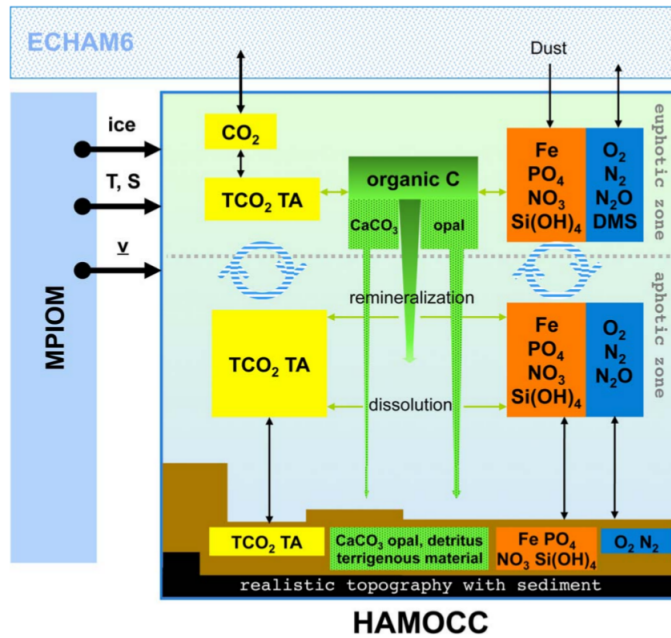


Figure 2: A schematic overview of the global ocean biogeochemistry model HAMOCC [Ilyina et al., 2013]

**misc/low impact on variability: chemistry, sediment** Other processes in a biogeochemical model act on longer timescales or small amplitude and hence lack a strong signal in the carbon cycle.

The chemistry in HAMOCC is modeled in the carbonate system and keeps track of alkalinity. Dissolved inorganic carbon and pH (\*check that\*) are directly calculated and other information derived from that.

For falling detritus, there exist two different parts: opal producing if silicate is available or calcium carbonate producing. Calcification then changes the alkalinity and carbon budget.

Once detritus reach the ocean floor, particulate matter enters the sediment and finally the burial layer. At the boundary of the sediment, all tracers are in exchange with the sediment which via pore water exchange [Heinze et al., 1991].

## 2.2 Large ensemble

**general: what is it? how produced technically?** Large ensemble simulation are a novel tool to investigate internal variability. By repeating a climate simulation with an identical forcing and model code but changing the initial conditions slightly, single ensemble members will be exposed to the same process implementations but the interplay at a stochastically random level lets each realisation evolve in a unique way while still being bound to a common forced trend.

The MPI-ESM Large Ensemble (MPI-ESM LE) contains 100 simulations under historical CMIP5 forcing from 1850 to 2005 and is extended under Representative Concentration Pathway (RCP) 4.5 scenario until 2100. Ensemble members differ through starting from different year of the pre-industrial control simulation, so ocean and atmosphere have different initial conditions in each run. This was achieved by branching off ensemble members from the control run after roughly 50 years by increasing the atmospheric pCO<sub>2</sub> levels.

MPI-ESM LE data already provided data to a few MPI-M publications, e.g. [Marotzke and Forster, 2015, Bittner et al., 2016].

**novel method: how are other ensembles different?** As large ensemble research is a recent feature due to powerful upscaling of super-computing facilities, the number of ensemble datasets is limited and published papers infrequent.

NCAR's Community Earth System Model large ensemble (CESM LE) [Kay et al., 2015] underlies the pioneering internal variability studies of Deser et al.. The initial state of the atmosphere was slightly perturbed by roundoff-level changes to air temperature in their 32 runs. CESM LE served for studies analyzing the timescales of detection of trend in the ocean carbon sink [McKinley et al., 2016] and the partitioning of its uncertainties [Lovenduski et al., 2016].

GFDL ran a 30-member ensemble simulation based on their model ESM2M. They use different dates separated by one day each but didn't publish any oceanic carbon uptake

paper [Rodgers et al., 2015].

Previous studies assume gaussian statistics, but lack an adequate ensemble size to check for in detail [Thompson et al., 2015, Deser et al., 2012] (see 17).

## 2.3 Data

**where are they from and why I choose this product?** For comparison of CO<sub>2</sub>flux with model simulations, I use the SOM-FFN data which is based on the Surface Ocean Atlas Version 4 (SOCATv4) [Landschützer et al., 2016]. It uses a neural network-based data interpolation to create pCO<sub>2</sub> maps [Landschützer et al., 2014]. The data product is smoothed by a 3x3 filter averaging two months and the neighboring grid cells, but this has little effect on seasonal dynamics. I use this pCO<sub>2</sub> data product because it seems a smart interpolation of pCO<sub>2</sub> data to cover regions without direct pCO<sub>2</sub> measurements. However, the input training data of the algorithm is seasonally biased, as the available pCO<sub>2</sub> samples originate mostly from austral summer months.

### 3 Historical evolution of the Southern Ocean carbon sink

carbon sink SO: forced trend and int variability, int var results explain fig. 3; Internal variability, defined as the  $1\sigma$ -spread of the 100-members, is constant over this period ( $0.18 \pm 0.02 \text{ PgC yr}^{-1}$ ). why can I do that:refer fig. 17

**comparison ensemble to data** SOM-FFN data ranges within the  $2\sigma$  ensemble spread. We find carbon trends similar to those in the 1990s and 2000s.

**choice of trends: compromise signal strength and signal monotonic length; describe selection technical** compromise between decade=10yrs vs interannual variability, not too strong influence of atmospheric forced trend and strength of signal Fig 18; Exemplary for all decadal carbon sink trend ensemble members, I show the most extreme cases. The underlying mechanisms for carbon sink trends in our ensemble simulation seem to be of the same origin regardless of the exact trend period.

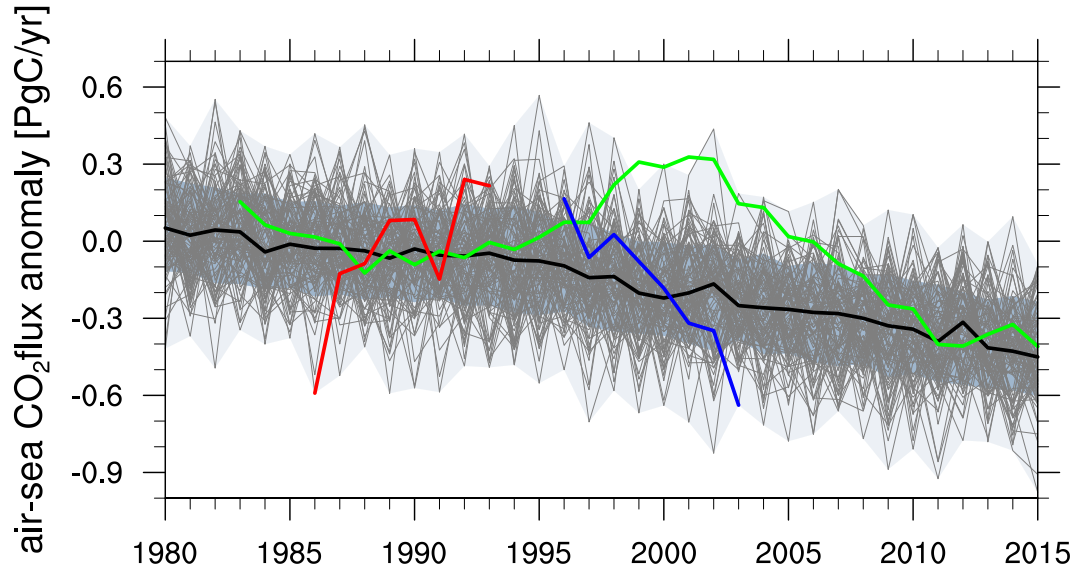


Figure 3: Evolution of the Southern Ocean carbon sink anomaly south of  $35^\circ\text{S}$ . Grey lines show the 100 ensemble members, the black line the ensemble median, the gray shading is the range of the ensemble, the blue shading is the  $1\sigma$  ensemble spread, the red line shows a positive sink trend, the blue line shows a negative sink trend, the green line represents the SOM-FFN observation-based estimate [Landschützer et al., 2015]; negative values indicate anomalous uptake with respect to the 1980s

**timeseries sam, biology, upwelling index? nice-to-have, but no connection to storyline; temporal results: seems short**

**transition to process understanding in spatial view; afterwards only two members shown exemplarily** As shown in previous studies [[Le Quéré et al., 2007](#)], the variations of oceanic carbon uptake are related to the background thermal and dynamic changes. Some note on biology referring to hypothesis?

## **4 Spatial distribution of Southern Ocean carbon sink**

**mean state and internal variability Southern ocean carbon sink** refer to fig. 4

**mean state and internal variability Southern ocean westerly winds?** no plot yet

**mean state and internal variability of biology and link to carbon sink** refer to fig. 4

**mean state and internal variability of upper ocean circulation and link to carbon sink** refer to fig. 5

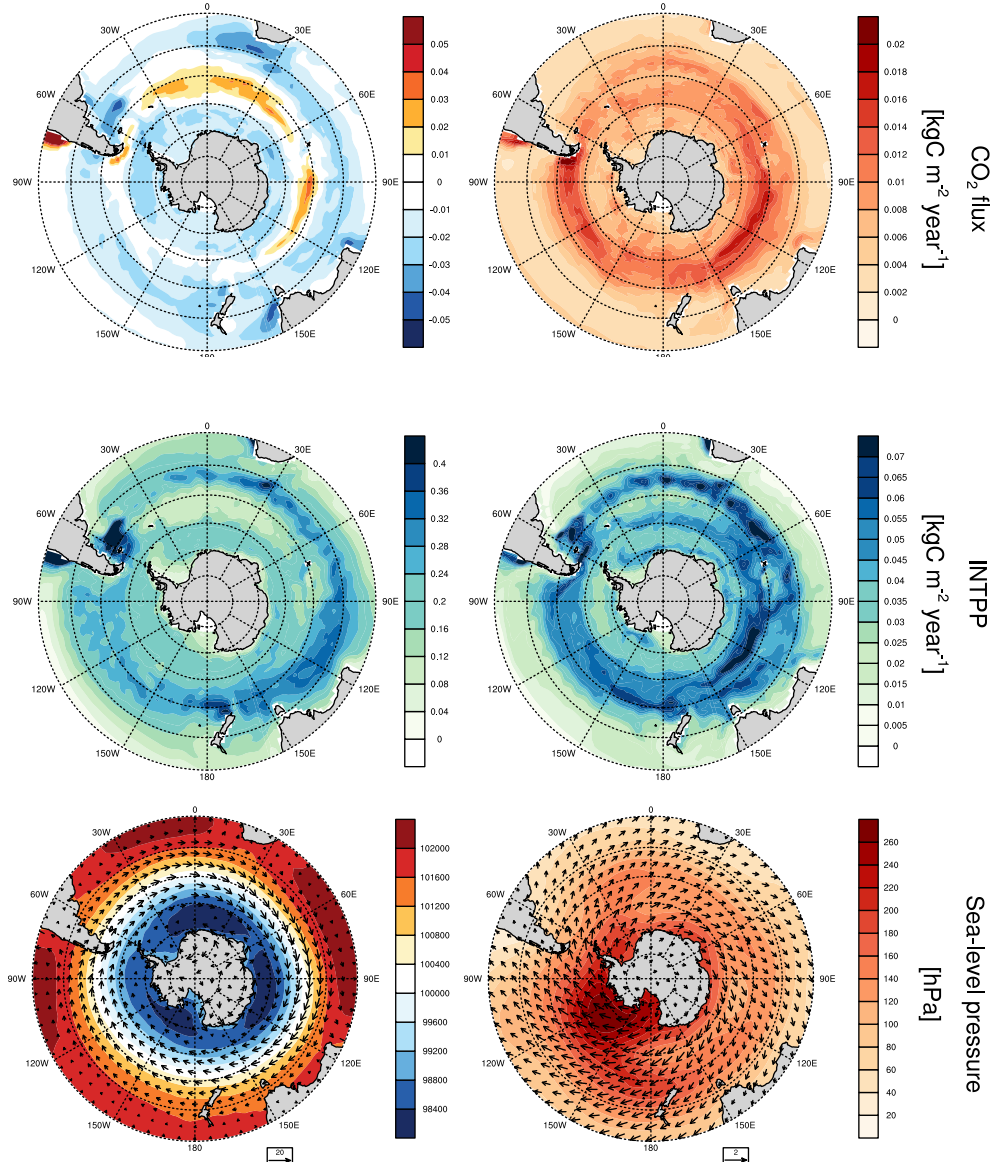


Figure 4: Spatial distribution of the yearmean Southern Ocean CO<sub>2</sub>flux (top) and primary production (bottom): negative values indicate ocean uptake ensemble median (left) as forced signal and ensemble standard deviation (right) as internal variability

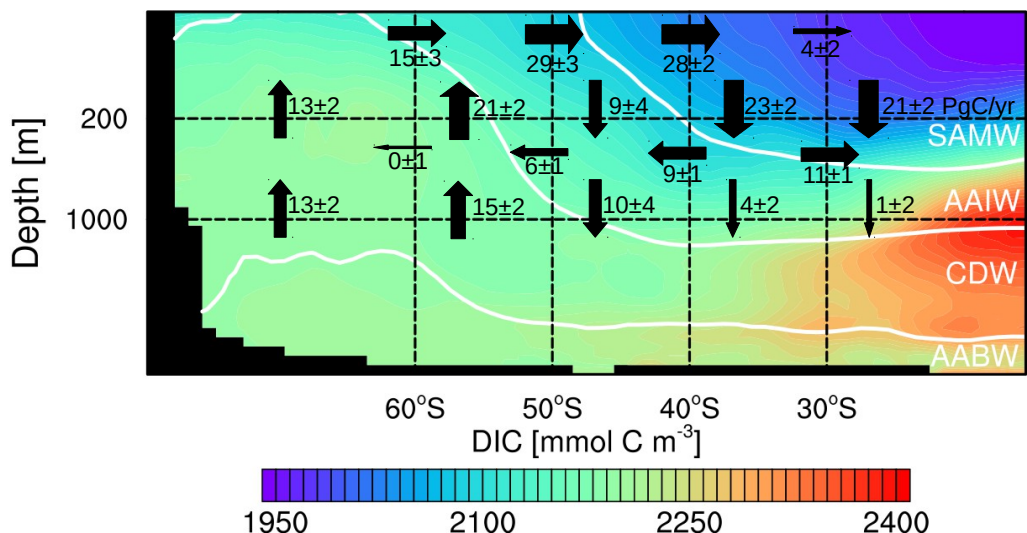


Figure 5: Upper-ocean overturning circulation modulates the carbon sink as carbon-rich water are upwelled and carbon-depleted water are downwelled; black arrows show yearly mean advective carbon transport; white lines are isopycnals separating Sub-Antarctic Mode Water (SAMW), Antarctic Intermediate Water (AAIW), Circumpolar Deep Water (CDW) and Antarctic Bottom Water (AABW)

## 4.1 Negative trends in carbon sink

**trends in pCO<sub>2</sub> and westerly winds** refer fig. 6

pCO<sub>2</sub> (and not co2flux) to show co2flux not only increasing due to stronger winds only by formula The region of 50-60°S has the strongest decreasing trend in CO<sub>2</sub>flux. leads to hypothesis

**schematics: explain carbon decrease due to wind** refer to fig. 7 - can I show this already here or better after the plots

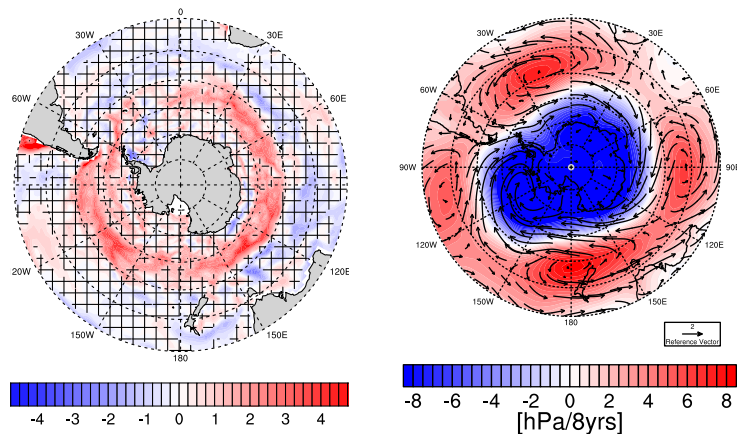


Figure 6: pCO<sub>2</sub>(right) (left) and Trends in sea-level pressure and winds - should I also discuss thermal and non-thermal trends in [Landschützer et al., 2015]?

### 4.1.1 Changes in biology in negative CO<sub>2</sub>flux trends

**on trends in co2flux, intpp** Primary production and CO<sub>2</sub>flux show opposing trend patterns as plankton growth takes up large amounts of surface DIC and hence lowers pCO<sub>2</sub>

**on intpp not increasing because of more nutrients** different than [Lovenduski and Gruber, 2005] (can I cite this here or only in discussion? or rather cite paper about SO iron lack and increased iron supply from upwelling?)

**on temp and light limitation changes due to SAM, coastal due to ice**

**then why intpp decreases in 50s? zmlld mixing and light depth limitation** Sverdrup [Sverdrup, 1953] introduced his concept of critical depth based turbulent mixing as a requirement for plankton blooms [Franks, 2014]

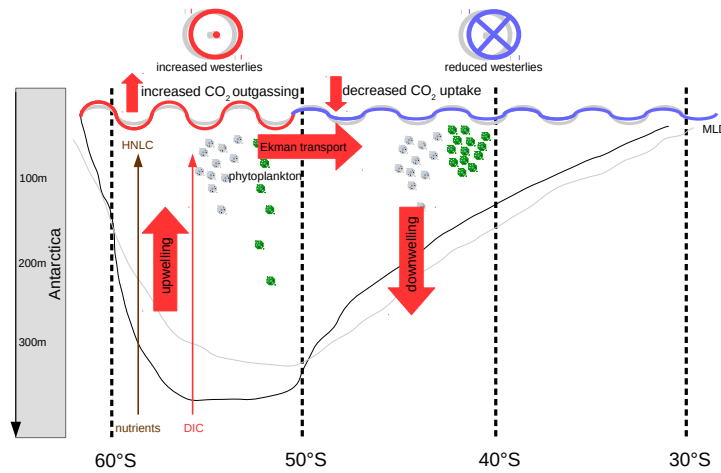


Figure 7: Schematic illustration of the Southern Ocean under the context of increasing westerly winds and response of biology and upper-ocean circulation towards the carbon sink

**center of mass of phytoplankton and wind penetration depth** refer fig. 8

**concentration increase of intpp at 40s due to advection/ekman transport** refer fig. 9

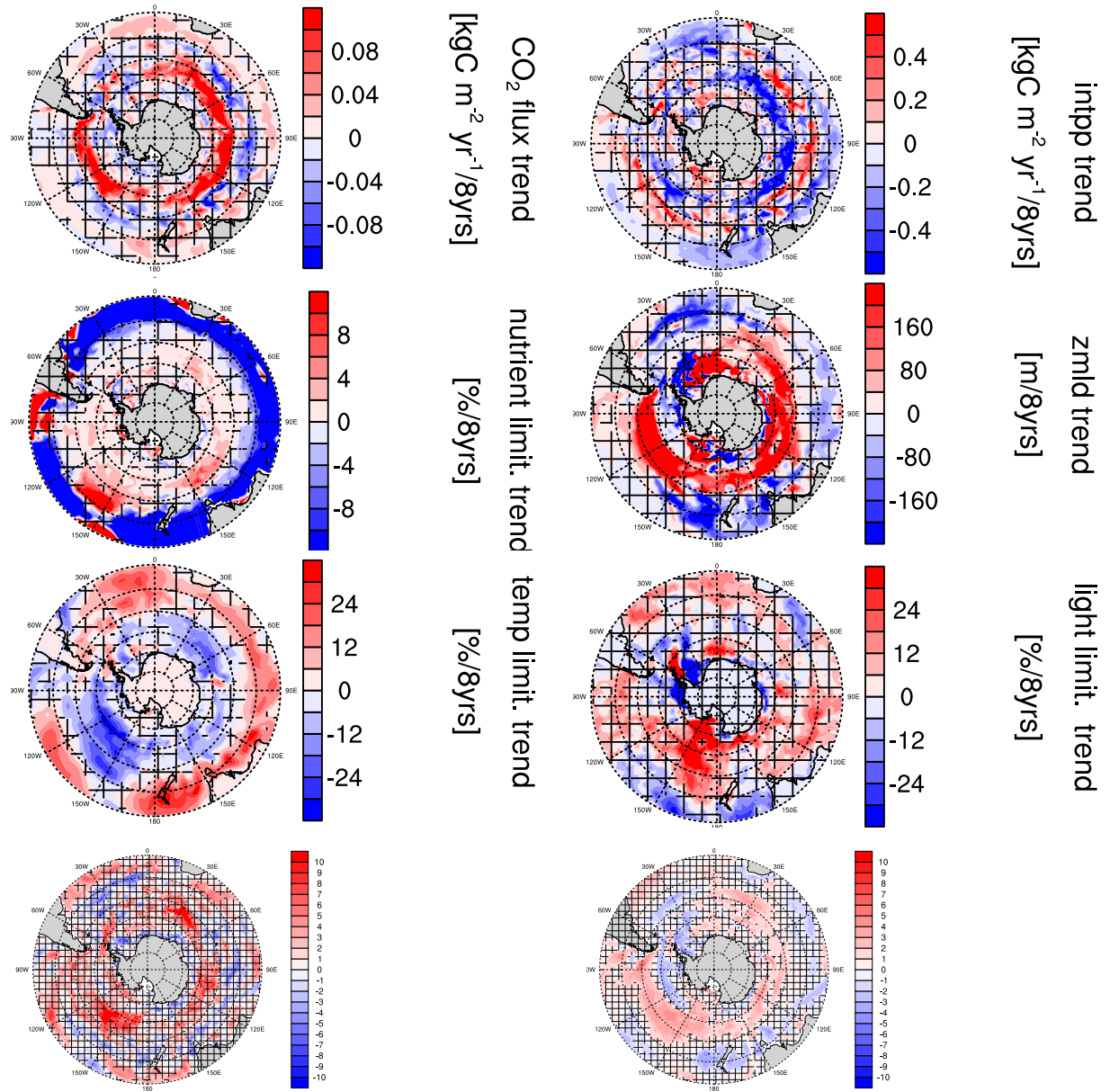


Figure 8: Southern Ocean austral summer trends per 8 years:  $\text{CO}_2$ flux (top left), vertically integrated primary production (top right), nutrient limitation (middle right), mixed layer depth (middle left), temperature limitation function (bottom left) and light limitation function (bottom right); Trends in [m/8yrs] for phytoplankton average depth (left) and average depth of vertical diffusivity due to wind (right); hatched areas indicate where trends were below 5% significance

#### 4.1.2 Changes in ocean circulation in negative CO<sub>2</sub>flux trends

**transition: zmlt trends; Upper-ocean overturning circulation: up, ekman transport, downwelling** The strong trend in MLD could also be a sign of increasing outgassing due to more mixing (fig. 8). refer to fig. 9 temperature pump effect?

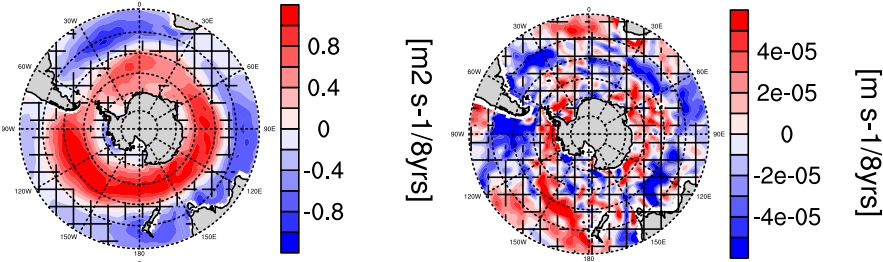


Figure 9: Ekman transport and ekman upwelling trends

**carbon transport changes** refer fig. 10

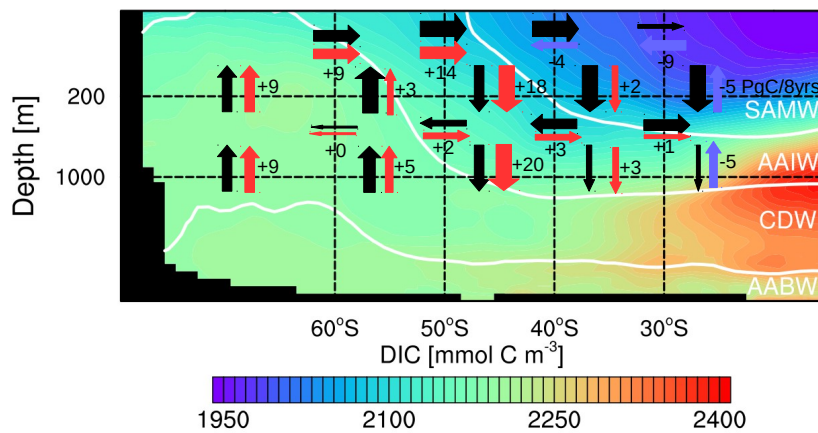


Figure 10: Increased upper-ocean overturning circulation weakens the carbon sink as carbon-rich water are upwelled and carbon-depleted water are downwelled

## 4.2 Positive trends in carbon sink

disclaimer: everything upside down

trends in pCO<sub>2</sub> and westerly winds refer fig. 11 The region of 50-60°S has the strongest decreasing trend in CO<sub>2</sub>flux. leads to hypothesis

schematic changes due to wind refer to fig. 12

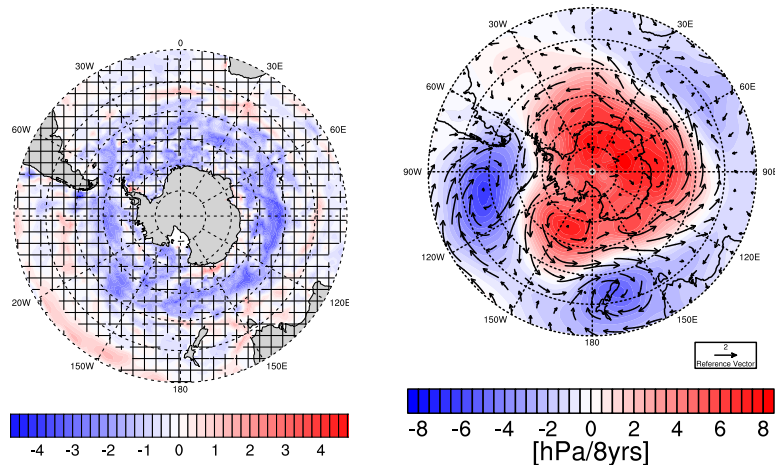


Figure 11: Trends in pCO<sub>2</sub> (left) and sea-level pressure and winds (right)

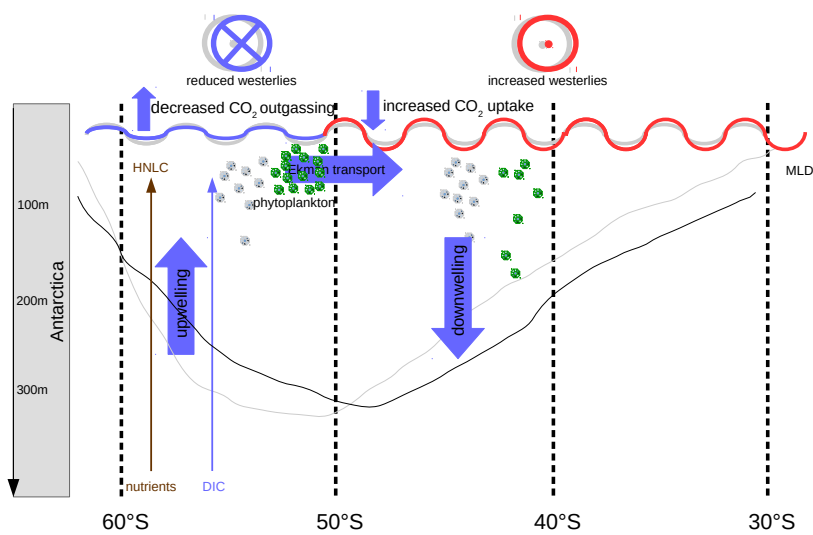


Figure 12: Schematic illustration of the Southern Ocean under the context of decreasing westerly winds

#### 4.2.1 Changes in biology in positive CO<sub>2</sub>flux trends

**on trends in co2flux, intpp** Primary production and CO<sub>2</sub>flux show opposing trend patterns as plankton growth takes up less surface DIC and hence pCO<sub>2</sub> increases fig. 11. refer to fig. 13

**on intpp not decreasing because of less nutrients** different than [[Lovenduski and Gruber, 2005](#)] (can I cite this here or only in discussion?)

**on temp and light limitation changes due to SAM, coastal due to ice**

the why intpp increases in 50s: using less zmld mixing refer fig. 13

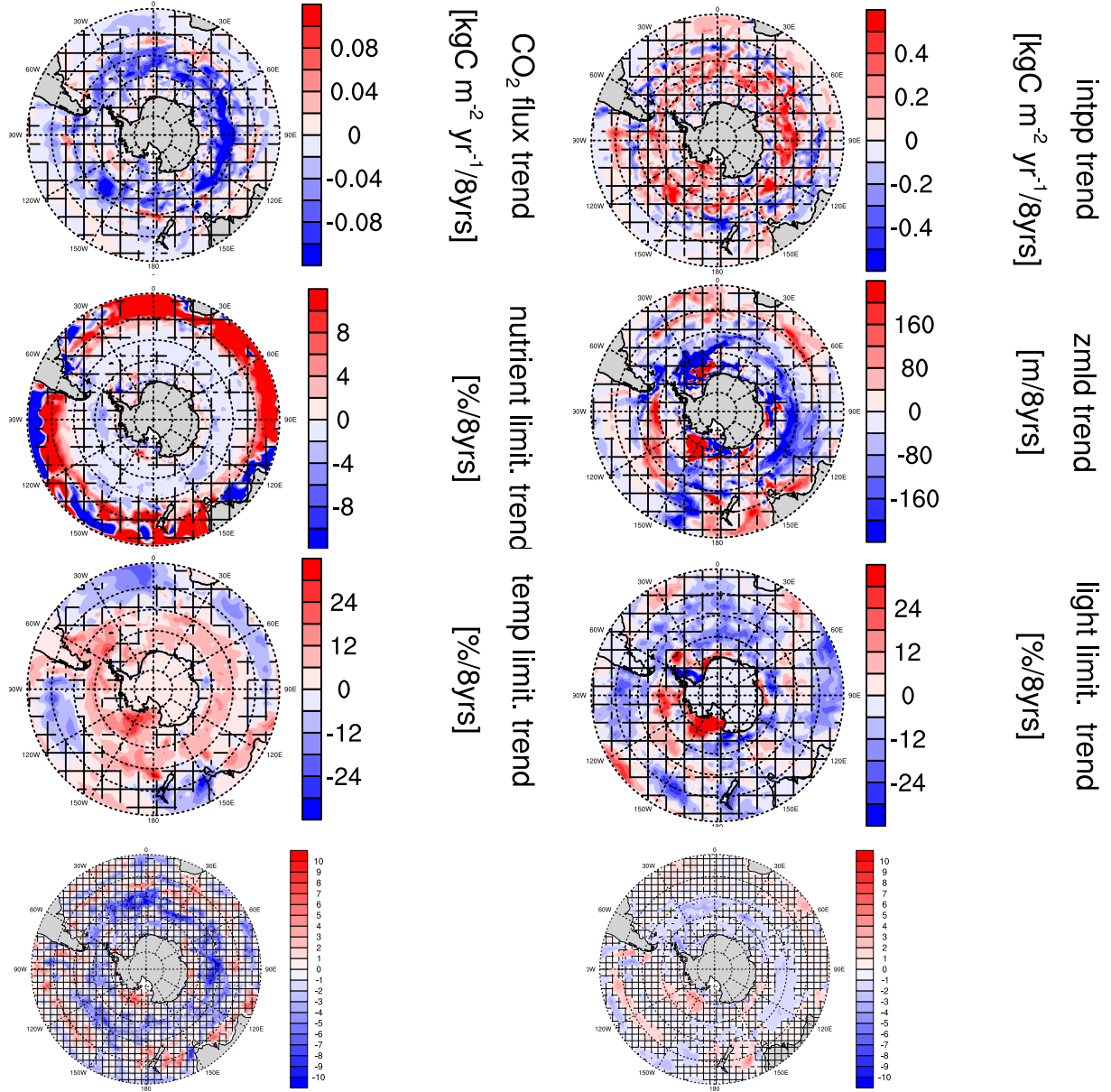


Figure 13: Southern Ocean austral summer trends per 8 years:  $\text{CO}_2$ flux (top left), vertically integrated primary production (top right), nutrient limitation (middle right), mixed layer depth (middle left), temperature limitation function (bottom left) and light limitation function (bottom right); Trends in [m/8yrs] for phytoplankton average depth (left) and average depth of vertical diffusivity due to wind (right); hatched areas indicate where trends were below 5% significance

#### 4.2.2 Changes in ocean circulation in positive CO<sub>2</sub>flux trends

**transition: zmlld trends; Upper-ocean overturning circulation: up, ekman transport, downwelling** The strong stabilizing trend in MLD could also be a sign of decreasing outgassing due to less mixing (fig. 13). refer to fig. 14 temperature pump effect?

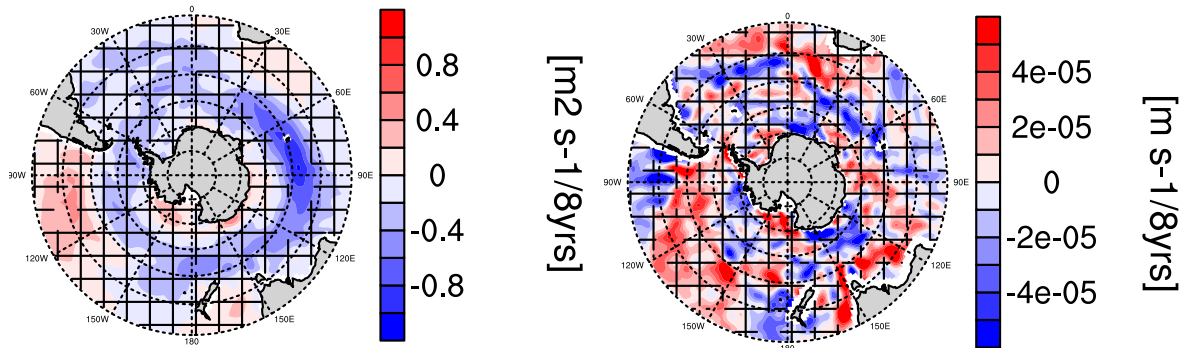


Figure 14: Ekman transport and ekman upwelling trends

**carbon transport changes** refer fig. 15

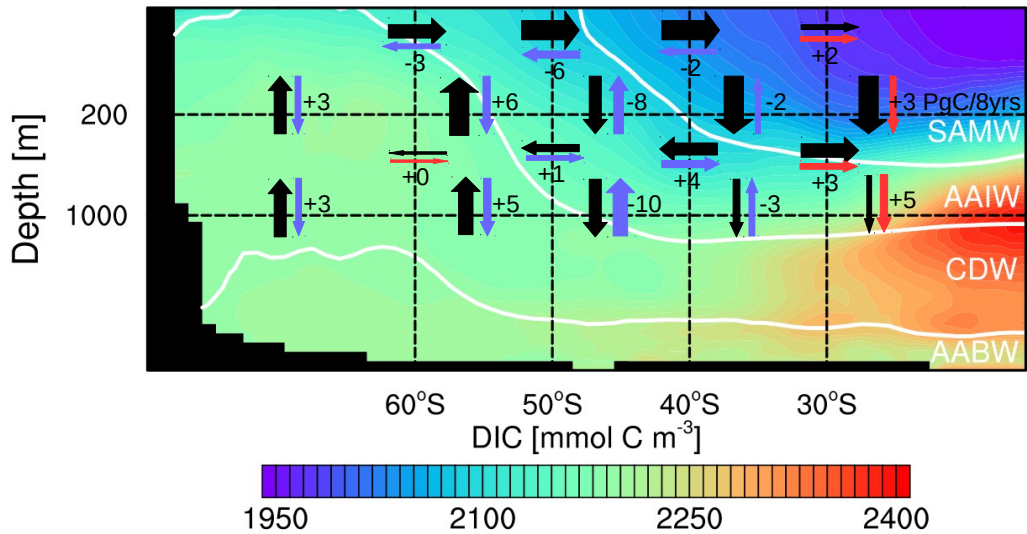


Figure 15: Decreased upper-ocean overturning circulation strengthens the carbon sink as carbon-rich water are less upwelled and carbon-depleted water are less downwelled - background is static and not this specific member, ok?

## 5 50-60S dominates Internal Variability of the total Southern Ocean carbon sink due to winds - need a better title: emphasis on 50S as driving int var region via winds

on area 50-60S as driver of Southern Ocean internal variability, correlation plots co2flux and wind trends fig. 16 refer to fig. 7 and fig. 12 stronger winds isopycnal movement [Lauderdale et al., 2013]  
co2flux trend =  $(0.081 \pm 0.001)$  SAM trend

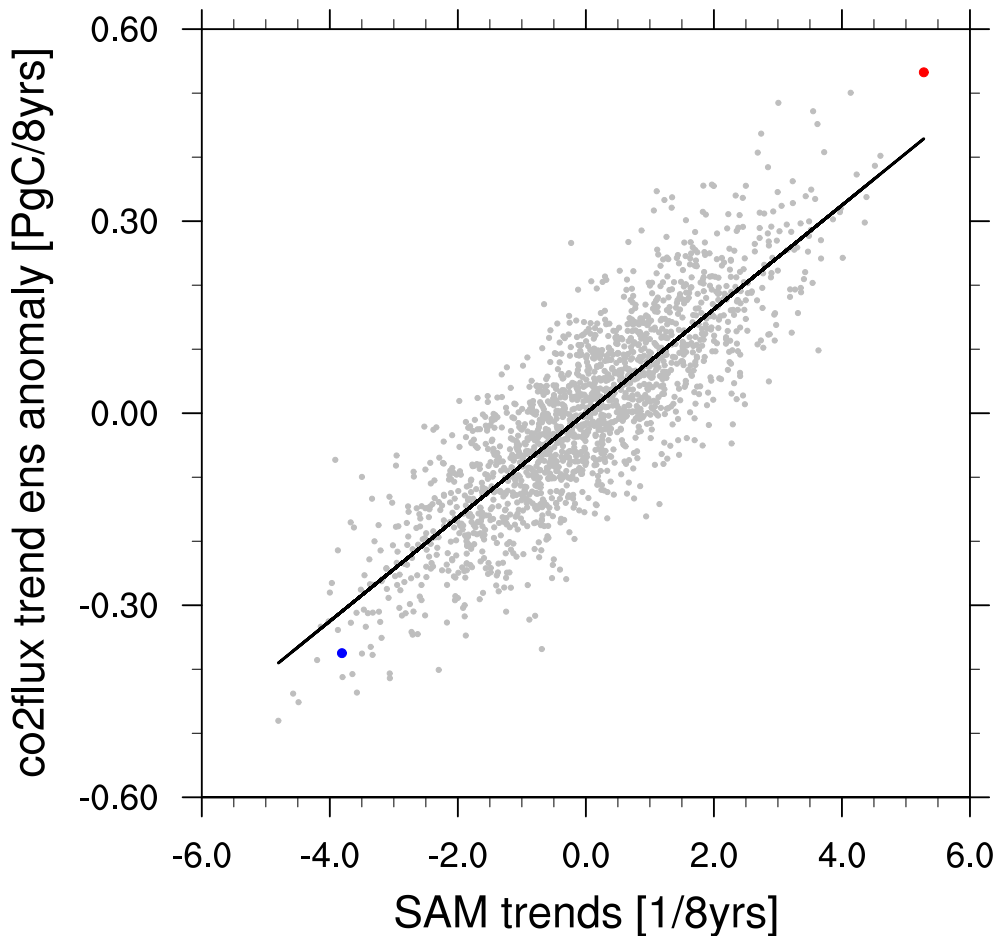


Figure 16: Southern Annular Mode (SAM) as indicator of wind strength vs. CO<sub>2</sub>flux south of 35°S; left 50-60s; right 40-50; one data point represents 8-year trends of single realization minus ensemble mean in 8-year periods between 1980 and 2005; green dot is negative trend example, red dot is positive trend example

## 6 estimate: bio vs upwelling

still have to come up with something like co2flux separation in [[Lauderdale et al., 2016](#)]; nice to have

## 7 Discussion

My results in perspective...

**Here I compare to other paper's messages (and results), in Results I only cite papers to emphasize processes**

**on comparison biology paper** Iron-hypothesis [Martin, 1990] doesn't apply to HAMOCC; similar zmlc co2flux response though location differs [Lovenduski and Gruber, 2005, Hauck et al., 2013, Wang and Moore, 2012]

**on comparison circulation paper** upwelling found to be major carbon sink driver [Landschützer et al., 2015, Le Quéré et al., 2007, Lovenduski et al., 2007], upwelling location boundaries differ slightly, upwelling trends deeper into ocean [DeVries et al., 2017]

idealised sensitivity studies of carbon due to wind changes [Lauderdale et al., 2013]

**on comparison earlier co2flux paper** trend in same order of magnitude reproduced; different 1980s anomaly [Le Quéré et al., 2007, Lovenduski et al., 2007, Landschützer et al., 2015] also reference to Sarmiento ARGO estimates: strength: insitu two years; weakness: few floats for large areas; SOM-FFN 2016 might be seasonally biased; interactive carbon cycle produces 25% higher internal variability [Ilyina et al., 2013]

**on internal variability comparison** US models have tropical and Indian Pacific as dominating variability mode region, MPI has Southern Ocean, MPI has higher int var than CESM, but lower than GFDL [Resplandy et al., 2015]

**on ensemble comparisons** CESM LE cannot reproduce decadal trends [private communication] weak SO carbon sink [McKinley et al., 2016]  
no knowledge about GFDL [Rodgers et al., 2015]

**on MPI-OM Southern Ocean performance evaluation papers** [Jungclaus et al., 2013, Sallée et al., 2013, Salle et al., 2013, Heuzé et al., 2013, Stössel et al., 2015]

**on HAMOCC SO performance** pCO<sub>2</sub> comparison Takahashi or surface DIC GLO-DAP [Ilyina et al., 2013]

amplified seasonal cycle [Nevison et al., 2016], early HAMOCC tuned for NH [Six and Maier-Reimer, 1996]

## 8 Summary and conclusions

**what I did and internal variability value ±** make sure three questions are answered

**two wind regimes of internal variability** processes processes at 50-60S linking to wind and summarising results of figure 16

**outlook: large ensemble variability modeling** Outlook paragraph on internal variability from large ensemble simulations; ICLE comparison Rodgers

**outlook: observational focus on Southern Ocean** ARGO data and SOM-FFN combined longer timeseries

## References and Notes

- M. Bittner, H. Schmidt, C. Timmreck, and F. Sienz. Using a large ensemble of simulations to assess the Northern Hemisphere stratospheric dynamical response to tropical volcanic eruptions and its uncertainty. *Geophysical Research Letters*, 43(17):9324–9332, 2016. ISSN 1944-8007. doi: 10.1002/2016GL070587. URL <http://dx.doi.org/10.1002/2016GL070587>. 2016GL070587.
- C. Deser, A. Phillips, V. Bourdette, and H. Teng. Uncertainty in climate change projections: the role of internal variability. *Clim Dyn*, 38(3-4):527–546, dec 2012. doi: 10.1007/s00382-010-0977-x. URL <http://dx.doi.org/10.1007/s00382-010-0977-x>.
- T. DeVries, M. Holzer, and F. Primeau. Recent increase in oceanic carbon uptake driven by weaker upper-ocean overturning. *Nature*, 542(7640):215–218, feb 2017. doi: 10.1038/nature21068. URL <https://doi.org/10.1038%2Fnature21068>.
- R. W. Eppley. Temperature and phytoplankton growth in the sea. *Fishery Bulletin*, 70(4):1063–1085, 1972.
- P. J. S. Franks. Has sverdrup’s critical depth hypothesis been tested? mixed layers vs. turbulent layers. *ICES Journal of Marine Science: Journal du Conseil*, 72(6):1897–1907, oct 2014. doi: 10.1093/icesjms/fsu175.
- P. R. Gent, J. Willebrand, T. J. McDougall, and J. C. McWilliams. Parameterizing eddy-induced tracer transports in ocean circulation models. *Journal of Physical Oceanography*, 25(4):463474, 1995. doi: 10.1175/1520-0485(1995)025<0463:PEITTI>2.0.CO;2. URL [http://dx.doi.org/10.1175/1520-0485\(1995\)025<0463:PEITTI>2.0.CO;2](http://dx.doi.org/10.1175/1520-0485(1995)025<0463:PEITTI>2.0.CO;2).
- M. A. Giorgetta, J. Jungclaus, C. H. Reick, S. Legutke, J. Bader, M. Böttinger, V. Brovkin, T. Crueger, M. Esch, K. Fieg, K. Glushak, V. Gayler, H. Haak, H.-D. Hollweg, T. Ilyina, S. Kinne, L. Kornblueh, D. Matei, T. Mauritsen, U. Mikolajewicz, W. Mueller, D. Notz, F. Pithan, T. Raddatz, S. Rast, R. Redler, E. Roeckner, H. Schmidt, R. Schnur, J. Segschneider, K. D. Six, M. Stockhouse, C. Timmreck, J. Wegner, H. Widmann, K.-H. Wieners, M. Claussen, J. Marotzke, and B. Stevens. Climate and carbon cycle changes from 1850 to 2100 in mpi-esm simulations for the coupled model intercomparison project phase 5. *Journal of Advances in Modeling*

- Earth Systems*, 5(3):572–597, 2013. ISSN 1942-2466. doi: 10.1002/jame.20038. URL <http://dx.doi.org/10.1002/jame.20038>.
- D. Gong and S. Wang. Definition of Antarctic Oscillation index. *Geophysical Research Letters*, 26(4):459–462, 1999. ISSN 1944-8007. doi: 10.1029/1999GL900003. URL <http://dx.doi.org/10.1029/1999GL900003>.
- J. Hauck, C. Völker, T. Wang, M. Hoppema, M. Losch, and D. A. Wolf-Gladrow. Seasonally different carbon flux changes in the southern ocean in response to the southern annular mode. *Global Biogeochemical Cycles*, 27(4):1236–1245, dec 2013. doi: 10.1002/2013gb004600. URL <http://dx.doi.org/10.1002/2013GB004600>.
- C. Heinze, E. Maier-Reimer, and K. Winn. Glacial pco<sub>2</sub> reduction by the world ocean: Experiments with the hamburg carbon cycle model. *Paleoceanography*, 6(4):395–430, 1991. ISSN 1944-9186. doi: 10.1029/91PA00489. URL <http://dx.doi.org/10.1029/91PA00489>.
- C. Heuzé, K. J. Heywood, D. P. Stevens, and J. K. Ridley. Southern ocean bottom water characteristics in CMIP5 models. *Geophys. Res. Lett.*, 40(7):1409–1414, apr 2013. doi: 10.1002/grl.50287. URL <http://dx.doi.org/10.1002/grl.50287>.
- T. Ilyina, K. D. Six, J. Segschneider, E. Maier-Reimer, H. Li, and I. Núñez-Riboni. Global ocean biogeochemistry model hamocc: Model architecture and performance as component of the mpi-earth system model in different cmip5 experimental realizations. *Journal of Advances in Modeling Earth Systems*, 5(2):287–315, 2013. ISSN 1942-2466. doi: 10.1029/2012MS000178. URL <http://dx.doi.org/10.1029/2012MS000178>.
- J. H. Jungclaus, N. Fischer, H. Haak, K. Lohmann, J. Marotzke, D. Matei, U. Mikolajewicz, D. Notz, and J. S. von Storch. Characteristics of the ocean simulations in the max planck institute ocean model (mpiom) the ocean component of the mpi-earth system model. *Journal of Advances in Modeling Earth Systems*, 5(2):422–446, 2013. ISSN 1942-2466. doi: 10.1002/jame.20023. URL <http://dx.doi.org/10.1002/jame.20023>.
- J. E. Kay, C. Deser, A. Phillips, A. Mai, C. Hannay, G. Strand, J. M. Arblaster, S. C. Bates, G. Danabasoglu, J. Edwards, M. Holland, P. Kushner, J.-F. Lamarque, D. Lawrence, K. Lindsay, A. Middleton, E. Munoz, R. Neale, K. Oleson, L. Polvani,

- and M. Vertenstein. The community earth system model (CESM) large ensemble project: A community resource for studying climate change in the presence of internal climate variability. *Bull. Amer. Meteor. Soc.*, 96(8):1333–1349, aug 2015. doi: 10.1175/bams-d-13-00255.1. URL <http://dx.doi.org/10.1175/BAMS-D-13-00255.1>.
- A. Kessler and J. Tjiputra. The southern ocean as a constraint to reduce uncertainty in future ocean carbon sinks. *Earth Syst. Dynam.*, 7(2):295–312, apr 2016. doi: 10.5194/esd-7-295-2016. URL <http://dx.doi.org/10.5194/esd-7-295-2016>.
- P. Landschützer, N. Gruber, D. C. E. Bakker, and U. Schuster. Recent variability of the global ocean carbon sink. *Global Biogeochemical Cycles*, 28(9):927–949, sep 2014. doi: 10.1002/2014gb004853. URL <http://dx.doi.org/10.1002/2014GB004853>.
- P. Landschützer, N. Gruber, F. A. Haumann, C. Rödenbeck, D. C. E. Bakker, S. van Heuven, M. Hoppema, N. Metzl, C. Sweeney, T. Takahashi, B. Tilbrook, and R. Wanninkhof. The reinvigoration of the southern ocean carbon sink. *Science*, 349(6253):1221–1224, 2015. ISSN 0036-8075. doi: 10.1126/science.aab2620. URL <http://science.sciencemag.org/content/349/6253/1221>.
- P. Landschützer, N. Gruber, and D. C. E. Bakker. Decadal variations and trends of the global ocean carbon sink. *Global Biogeochemical Cycles*, 30(10):1396–1417, oct 2016. doi: 10.1002/2015gb005359. URL <https://doi.org/10.1002%2F2015gb005359>.
- J. M. Lauderdale, A. C. N. Garabato, K. I. C. Oliver, M. J. Follows, and R. G. Williams. Wind-driven changes in southern ocean residual circulation, ocean carbon reservoirs and atmospheric co<sub>2</sub>. *Climate Dynamics*, 41(7):2145–2164, 2013. ISSN 1432-0894. doi: 10.1007/s00382-012-1650-3. URL <http://dx.doi.org/10.1007/s00382-012-1650-3>.
- J. M. Lauderdale, S. Dutkiewicz, R. G. Williams, and M. J. Follows. Quantifying the drivers of ocean-atmosphere CO<sub>2</sub> fluxes. *Global Biogeochem. Cycles*, 2016. doi: 10.1002/2016gb005400. URL <http://dx.doi.org/10.1002/2016GB005400>.
- C. Le Quéré, C. Rödenbeck, E. T. Buitenhuis, T. J. Conway, R. Langenfelds, A. Gomez, C. Labuschagne, M. Ramonet, T. Nakazawa, N. Metzl, N. Gillett, and M. Heimann. Saturation of the southern ocean co<sub>2</sub> sink due to recent climate change. *Science*, 316(5832):1735–1738, 2007. ISSN 0036-8075. doi: 10.1126/science.1136188. URL <http://science.sciencemag.org/content/316/5832/1735>.

C. Le Quéré, R. M. Andrew, J. G. Canadell, S. Sitch, J. I. Korsbakken, G. P. Peters, A. C. Manning, T. A. Boden, P. P. Tans, R. A. Houghton, R. F. Keeling, S. Alin, O. D. Andrews, P. Anthoni, L. Barbero, L. Bopp, F. Chevallier, L. P. Chini, P. Ciais, K. Currie, C. Delire, S. C. Doney, P. Friedlingstein, T. Gkritzalis, I. Harris, J. Hauck, V. Haverd, M. Hoppema, K. K. Goldewijk, A. K. Jain, E. Kato, A. Kötzinger, P. Landschützer, N. Lefèvre, A. Lenton, S. Lienert, D. Lombardozzi, J. R. Melton, N. Metzl, F. Millero, P. M. S. Monteiro, D. R. Munro, J. E. M. S. Nabel, S. Nakaoka, K. O'Brien, A. Olsen, A. M. Omar, T. Ono, D. Pierrot, B. Poulter, C. Rödenbeck, J. Salisbury, U. Schuster, J. Schwinger, R. Séférian, I. Skjelvan, B. D. Stocker, A. J. Sutton, T. Takahashi, H. Tian, B. Tilbrook, I. T. van der Laan-Luijkx, G. R. van der Werf, N. Viovy, A. P. Walker, A. J. Wiltshire, and S. Zaehle. Global carbon budget 2016. *Earth System Science Data*, 8(2):605–649, nov 2016. doi: 10.5194/essd-8-605-2016. URL <http://dx.doi.org/10.5194/essd-8-605-2016>.

N. S. Lovenduski and N. Gruber. Impact of the southern annular mode on southern ocean circulation and biology. *Geophys. Res. Lett.*, 32(L11603), 2005. doi: 10.1029/2005GL022727. URL <http://onlinelibrary.wiley.com/doi/10.1029/2005GL022727/pdf>.

N. S. Lovenduski, N. Gruber, S. C. Doney, and I. D. Lima. Enhanced co<sub>2</sub> outgassing in the southern ocean from a positive phase of the southern annular mode. *Global Biogeochemical Cycles*, 21(2):n/a–n/a, 2007. ISSN 1944-9224. doi: 10.1029/2006GB002900. URL <http://dx.doi.org/10.1029/2006GB002900>. GB2026.

N. S. Lovenduski, G. A. McKinley, A. R. Fay, K. Lindsay, and M. C. Long. Partitioning uncertainty in ocean carbon uptake projections: Internal variability, emission scenario, and model structure. *Global Biogeochemical Cycles*, 30(9):1276–1287, sep 2016. doi: 10.1002/2016gb005426. URL <http://dx.doi.org/10.1002/2016gb005426>.

J. Marotzke and P. M. Forster. Forcing, feedback and internal variability in global temperature trends. *Nature*, 517(7536):565–570, jan 2015. doi: 10.1038/nature14117. URL <http://dx.doi.org/10.1038/nature14117>.

S. Marsland, H. Haak, J. Jungclaus, M. Latif, and F. Röske. The max-planck-institute global ocean/sea ice model with orthogonal curvilinear coordinates. *Ocean Modelling*, 5(2):91 – 127, 2003. ISSN 1463-5003. doi: <http://dx.doi.org/10.1016/>

S1463-5003(02)00015-X. URL <http://www.sciencedirect.com/science/article/pii/S146350030200015X>.

J. H. Martin. Glacial-interglacial CO<sub>2</sub> change: The Iron Hypothesis. *Paleoceanography*, 5(1):1–13, 1990. ISSN 1944-9186. doi: 10.1029/PA005i001p00001. URL <http://dx.doi.org/10.1029/PA005i001p00001>.

G. A. McKinley, D. J. Pilcher, A. R. Fay, K. Lindsay, M. C. Long, and N. S. Lovenduski. Timescales for detection of trends in the ocean carbon sink. *Nature*, 530(7591):469–472, feb 2016. doi: 10.1038/nature16958. URL <http://dx.doi.org/10.1038/nature16958>.

C. D. Nevison, M. Manizza, R. F. Keeling, B. B. Stephens, J. D. Bent, J. Dunne, T. Ilyina, M. Long, L. Resplandy, J. Tjiputra, and S. Yukimoto. Evaluating CMIP5 ocean biogeochemistry and southern ocean carbon uptake using atmospheric potential oxygen: Present-day performance and future projection. *Geophys. Res. Lett.*, 43(5):2077–2085, mar 2016. doi: 10.1002/2015gl067584. URL <http://dx.doi.org/10.1002/2015GL067584>.

R. C. Pacanowski and S. G. H. Philander. Parameterization of Vertical Mixing in Numerical Models of Tropical Oceans. *Journal of Physical Oceanography*, 11(11):1443–1451, 1981. doi: 10.1175/1520-0485(1981)011<1443:POVMIN>2.0.CO;2. URL [http://dx.doi.org/10.1175/1520-0485\(1981\)011<1443:POVMIN>2.0.CO;2](http://dx.doi.org/10.1175/1520-0485(1981)011<1443:POVMIN>2.0.CO;2).

L. Resplandy, R. Séférian, and L. Bopp. Natural variability of CO<sub>2</sub> and O<sub>2</sub> fluxes: What can we learn from centuries-long climate models simulations? *Journal of Geophysical Research: Oceans*, 120(1):384–404, jan 2015. doi: 10.1002/2014jc010463. URL <https://doi.org/10.1002%2F2014jc010463>.

K. B. Rodgers, J. Lin, and T. L. Frlicher. Emergence of multiple ocean ecosystem drivers in a large ensemble suite with an earth system model. *Biogeosciences*, 12(11):3301–3320, jun 2015. doi: 10.5194/bg-12-3301-2015. URL <https://doi.org/10.5194%2Fbg-12-3301-2015>.

C. L. Sabine, R. A. Feely, N. Gruber, R. M. Key, K. Lee, J. L. Bullister, R. Wanninkhof, C. S. Wong, D. W. R. Wallace, B. Tilbrook, F. J. Millero, T.-H. Peng, A. Kozyr,

- T. Ono, and A. F. Rios. The oceanic sink for anthropogenic co<sub>2</sub>. *Science*, 305(5682):367–371, 2004. ISSN 0036-8075. doi: 10.1126/science.1097403. URL <http://science.scienmag.org/content/305/5682/367>.
- J.-B. Sallée, E. Shuckburgh, N. Bruneau, A. J. S. Meijers, T. J. Bracegirdle, and Z. Wang. Assessment of southern ocean mixed-layer depths in CMIP5 models: Historical bias and forcing response. *J. Geophys. Res. Oceans*, 118(4):1845–1862, apr 2013. doi: 10.1002/jgrc.20157. URL <http://dx.doi.org/10.1002/jgrc.20157>.
- J.-B. Salle, E. Shuckburgh, N. Bruneau, A. J. S. Meijers, T. J. Bracegirdle, Z. Wang, and T. Roy. Assessment of southern ocean water mass circulation and characteristics in cmip5 models: Historical bias and forcing response. *Journal of Geophysical Research: Oceans*, 118(4):1830–1844, 2013. ISSN 2169-9291. doi: 10.1002/jgrc.20135. URL <http://dx.doi.org/10.1002/jgrc.20135>.
- K. D. Six and E. Maier-Reimer. Effects of plankton dynamics on seasonal carbon fluxes in an ocean general circulation model. *Global Biogeochemical Cycles*, 10(4):559–583, 1996. ISSN 1944-9224. doi: 10.1029/96GB02561. URL <http://dx.doi.org/10.1029/96GB02561>.
- E. L. Smith. Photosynthesis in relation to light and carbon dioxide. *Proc. Nat. Acad. Sci.*, 22:504–511, 1936.
- B. Stevens, M. Giorgetta, M. Esch, T. Mauritsen, T. Crueger, S. Rast, M. Salzmann, H. Schmidt, J. Bader, K. Block, R. Brokopf, I. Fast, S. Kinne, L. Kornblueh, U. Lohmann, R. Pincus, T. Reichler, and E. Roeckner. Atmospheric component of the MPI-M Earth System Model: ECHAM6. *Journal of Advances in Modeling Earth Systems*, 5(2):146–172, 2013. ISSN 1942-2466. doi: 10.1002/jame.20015. URL <http://dx.doi.org/10.1002/jame.20015>.
- A. Stössel, D. Notz, F. A. Haumann, H. Haak, J. Jungclaus, and U. Mikolajewicz. Controlling high-latitude southern ocean convection in climate models. *Ocean Modelling*, 86: 58 – 75, 2015. ISSN 1463-5003. doi: <http://dx.doi.org/10.1016/j.ocemod.2014.11.008>. URL <http://www.sciencedirect.com/science/article/pii/S1463500314001760>.
- H. U. Sverdrup. On conditions for the vernal blooming of phytoplankton. *Journal du Conseil International pour l'Exploration de la Mer*, 18:287–295, 1953.

- K. E. Taylor, R. J. Stouffer, and G. A. Meehl. An overview of CMIP5 and the experiment design. *Bull. Amer. Meteor. Soc.*, 93(4):485–498, apr 2012. doi: 10.1175/bams-d-11-00094.1. URL <http://dx.doi.org/10.1175/BAMS-D-11-00094.1>.
- D. Thompson and J. Wallace. Annular modes in the extratropical circulation. part i: Month-month variability. *Journal of Climate*, 13(5):1000–1016, 2000. doi: 10.1175/1520-0442(2000)013<1000:AMITEC>2.0.CO;2. URL <http://journals.ametsoc.org/doi/pdf/10.1175/1520-0442%282000%29013%3C1040%3AR%3E2.0.CO%3B2>.
- D. W. J. Thompson, E. A. Barnes, C. Deser, W. E. Foust, and A. S. Phillips. Quantifying the role of internal climate variability in future climate trends. *Journal of Climate*, 28(16):6443–6456, aug 2015. doi: 10.1175/jcli-d-14-00830.1. URL <http://dx.doi.org/10.1175/JCLI-D-14-00830.1>.
- T. Volk and M. I. Hoffert. *Ocean Carbon Pumps: Analysis of Relative Strengths and Efficiencies in Ocean-Driven Atmospheric CO<sub>2</sub> Changes*, pages 99–110. American Geophysical Union, 1985. ISBN 9781118664322. doi: 10.1029/GM032p0099. URL <http://dx.doi.org/10.1029/GM032p0099>.
- S. Wang and J. K. Moore. Variability of primary production and air-sea CO<sub>2</sub> flux in the Southern Ocean. *Global Biogeochemical Cycles*, 26(1):n/an/a, 2012. ISSN 1944-9224. doi: 10.1029/2010GB003981. URL <http://dx.doi.org/10.1029/2010GB003981>. GB1008.
- R. Wanninkhof. Relationship between wind speed and gas exchange over the ocean. *Journal of Geophysical Research: Oceans*, 97(C5):7373–7382, 1992. ISSN 2156-2202. doi: 10.1029/92JC00188. URL <http://dx.doi.org/10.1029/92JC00188>.
- R. Wanninkhof, A. Oceanographic, M. Laboratory, and A. of. Relationship between wind speed and gas exchange over the ocean, revisited, 2013.
- R. Weiss. Carbon dioxide in water and seawater: the solubility of a non-ideal gas. *Marine Chemistry* 2, 2:203–215, 1974. doi: doi:10.1016/0304-4203(74)90015-2. URL <http://www.sciencedirect.com/science/article/pii/0304420374900152>.

## List of Figures

1	Schematic overview on the different components in MPI-Earth-System-Model with a diagnostic carbon cycle [Giorgetta et al., 2013] . . . . .	4
2	A schematic overview of the global ocean biogeochemistry model HAMOCC [Ilyina et al., 2013] . . . . .	6
3	Evolution of the Southern Ocean carbon sink anomaly south of 35°S. Grey lines show the 100 ensemble members, the black line the ensemble median, the gray shading is the range of the ensemble, the blue shading is the $1\sigma$ ensemble spread, the red line shows a positive sink trend, the blue line shows a negative sink trend, the green line represents the SOM-FFN observation-based estimate [Landschützer et al., 2015]; negative values indicate anomalous uptake with respect to the 1980s . . . . .	9
4	Spatial distribution of the yearmean Southern Ocean CO <sub>2</sub> flux (top) and primary production (bottom): negative values indicate ocean uptake ensemble median (left) as forced signal and ensemble standard deviation (right) as internal variability . . . . .	12
5	Upper-ocean overturning circulation modulates the carbon sink as carbon-rich water are upwelled and carbon-depleted water are downwelled; black arrows show yearly mean advective carbon transport; white lines are isopycnals separating Sub-Antarctic Mode Water (SAMW), Antarctic Intermediate Water (AAIW), Circumpolar Deep Water (CDW) and Antarctic Bottom Water (AABW) . . . . .	13
6	pCO <sub>2</sub> (right) (left) and Trends in sea-level pressure and winds - should I also discuss thermal and non-thermal trends in [Landschützer et al., 2015]? . . . . .	14
7	Schematic illustration of the Southern Ocean under the context of increasing westerly winds and response of biology and upper-ocean circulation towards the carbon sink . . . . .	15

8	Southern Ocean austral summer trends per 8 years: CO <sub>2</sub> flux (top left), vertically integrated primary production (top right), nutrient limitation (middle right), mixed layer depth (middle left), temperature limitation function (bottom left) and light limitation function (bottom right); Trends in [m/8yrs] for phytoplankton average depth (left) and average depth of vertical diffusivity due to wind (right); hatched areas indicate where trends were below 5% significance . . . . .	16
9	Ekman transport and ekman upwelling trends . . . . .	17
10	Increased upper-ocean overturning circulation weakens the carbon sink as carbon-rich water are upwelled and carbon-depleted water are downwelled .	17
11	Trends in pCO <sub>2</sub> (left) and sea-level pressure and winds (right) . . . . .	18
12	Schematic illustration of the Southern Ocean under the context of decreasing westerly winds . . . . .	18
13	Southern Ocean austral summer trends per 8 years: CO <sub>2</sub> flux (top left), vertically integrated primary production (top right), nutrient limitation (middle right), mixed layer depth (middle left), temperature limitation function (bottom left) and light limitation function (bottom right); Trends in [m/8yrs] for phytoplankton average depth (left) and average depth of vertical diffusivity due to wind (right); hatched areas indicate where trends were below 5% significance . . . . .	20
14	Ekman transport and ekman upwelling trends . . . . .	21
15	Decreased upper-ocean overturning circulation strengthens the carbon sink as carbon-rich water are less upwelled and carbon-depleted water are less downwelled - background is static and not this specific member, ok? . . . . .	21
16	Southern Annular Mode (SAM) as indicator of wind strength vs. CO <sub>2</sub> flux south of 35°S; left 50-60s; right 40-50; one data point represents 8-year trends of single realization minus ensemble mean in 8-year periods between 1980 and 2005; green dot is negative trend example, red dot is positive trend example . . . . .	22
17	Southern Ocean carbon sink: yearmean fieldsum 35-90S (left) and yearmean in a random grid cell (right) . . . . .	35
18	Southern Ocean carbon sink trends per trendlength; (above) normal; (below) detrended from ensmean trend . . . . .	36

## Supplementary information

### Statistics of Southern Ocean carbon sink

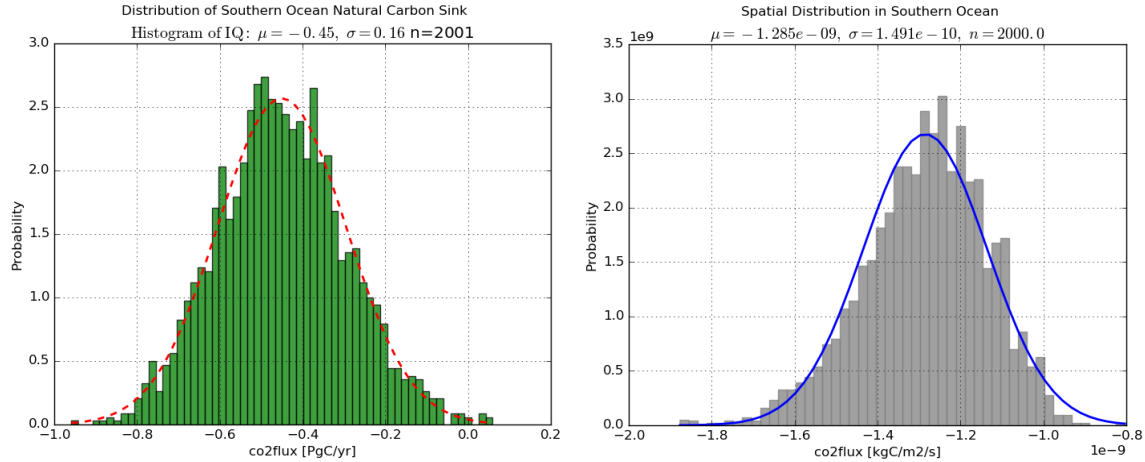


Figure 17: Southern Ocean carbon sink: yearmean fieldsum 35-90S (left) and yearmean in a random grid cell (right)

## CO<sub>2</sub>flux trends heatmap in MPI-ESM Large Ensemble

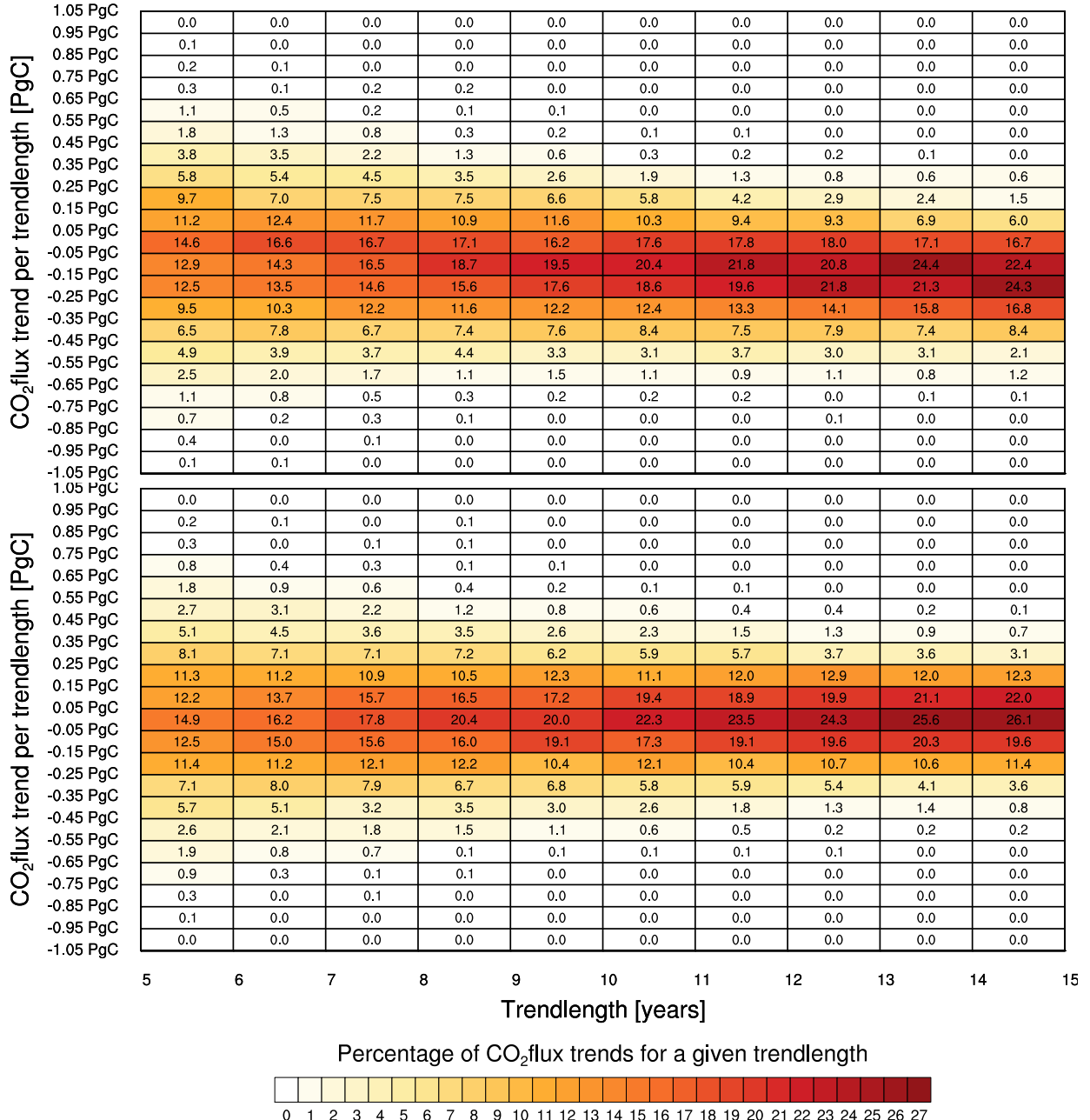


Figure 18: Southern Ocean carbon sink trends per trendlength; (above) normal; (below) detrended from ensmean trend